Journal of
Applied Crystallography

ISSN 1600-5767

Received 18 November 2014
Accepted 27 January 2015

Achieving grazing-incidence ultra-small-angle X-ray scattering in a laboratory setup

Nan Zheng,[a,b] Zhiyong Yi,[a,b] Zhenzhen Li,[a,b] Ran Chen,[a,b] Yuqing Lai[a]* and Yongfeng Men[a]*

[a]State Key Laboratory of Polymer Physics and Chemistry, Changchun Institute of Applied Chemistry, Chinese Academy of Sciences, Renmin Street 5625, Changchun, 130022, People's Republic of China, and [b]Dutch Polymer Institute (DPI), PO Box 902, Eindhoven, 5600 AX, The Netherlands. Correspondence e-mail: ylai@ciac.ac.cn, men@ciac.ac.cn

A grazing-incidence sample stage was designed for realizing grazing-incidence scattering measurements, especially in the ultra-small-angle regime, in a modified Xenocs Xeuss system in the laboratory. The designed sample stage, which is composed of four separate motorized positioning stages, allows the sample to be moved along four different directions to locate it in the proper position for scattering measurement. In an effort to realize grazing-incidence ultra-small-angle scattering (GIUSAXS) measurements, both the separation of the collimation slit systems and the sample-to-detector distance have been lengthened. At a separation of the collimation slit systems of 2400 mm and a sample-to-detector distance of 6558 mm, the effective smallest scattering vector magnitude $q_{\rm min}$ reaches 0.01 nm^{-1}. A colloidal crystalline thin film obtained from drying a polystyrene latex dispersion on silicon substrate was measured in the setup in GIUSAXS mode at different beam sizes. The resultant GIUSAXS patterns at smaller beam sizes reveal fine crystalline structures in the film.

1. Introduction

Thin films with sub-micrometre structural features are attracting more and more interest for basic research and with respect to their applications (Russell, 2002). Among many techniques that are used for the analysis of nanostructures, the small-angle X-ray scattering (SAXS) technique is a widely used one with many advantages. It is a nondestructive method and, because of the large probing volume, has excellent sampling statistics (Levine *et al.*, 1989; Naudon & Thiaudiere, 1997; Renaud *et al.*, 2009). In conventional SAXS mode, the beam passes through a bulk sample, detecting the fluctuation of electron density. SAXS combined with a reflection setup can be used to investigate thin films and surfaces using the grazing-incidence small-angle X-ray scattering (GISAXS) technique (Altamura, De Caro *et al.*, 2012; Holy & Baumbach, 1994; Salditt *et al.*, 1995; Müller-Buschbaum *et al.*, 1998, 2002; Müller-Buschbaum & Stamm, 1998; Müller-Buschbaum, 2003; Roth *et al.*, 2003). Compared to SAXS mode, the X-ray beam in GISAXS mode hits the sample with a very small incident angle (usually smaller than 1°), exploiting the finite penetration depth of totally reflected X-rays into the material; this geometry is extremely surface sensitive and allows us to investigate thin films down to the nanometre scale in thickness (Müller-Buschbaum *et al.*, 1999, 2000). Because high brilliance and collimation of the X-ray beam are required, most *in situ* GISAXS experiments are performed at synchrotron radiation facilities, such as SSRF, BSRF and DESY (Roth *et al.*, 2007; Papadakis *et al.*, 2008; Di *et al.*, 2010; Cheng *et al.*, 2011; You *et al.*, 2011; Zhong *et al.*, 2011, 2013; Zhang *et al.*, 2013, 2014*a*, 2014*b*; Zhao *et al.*, 2014). Much work on modified synchrotron GISAXS facilities has been reported (Roth *et al.*, 2006; Jerkily *et al.*, 2013; Ogawa *et al.*, 2013; Li *et al.*, 2014). Recently, *ex situ* GISAXS experiments for measuring static structures of thin films have become available in the laboratory owing to the development of new-generation microsource X-ray generators (Altamura, Lassandro *et al.*, 2012; Altamura, Holy *et al.*, 2012; Altamura, Sibillano *et al.*, 2012; De Caro *et al.*, 2012; Magliulo *et al.*, 2014; Mele *et al.*, 2012). Yet, research papers on laboratory grazing-incidence ultra-small-angle X-ray scattering (GIUSAXS) apparatus are rarely seen. GIUSAXS with an achievable scattering vector magnitude q down to 0.01 nm^{-1} has been only available at very long sample-to-detector distances at synchrotron beamlines (Hu *et al.*, 2009).

In this work, laboratory GIUSAXS experiments based on a modified Xenocs Xeuss small-angle X-ray scattering setup are reported. A four-direction motorized positioning sample stage was designed. By varying the beam size, we achieved high-resolution GIUSAXS patterns, indicating hidden crystalline ordering in a colloidal crystalline thin latex film. Our results showed experimentally the crucial role of beam size on the spatial resolution of the scattering pattern in the GIUSAXS geometry.

2. Concept and design

2.1. Background

In a GIUSAXS measurement, the position of the specular peak, *e.g.* the reflected beam point, may differ from sample to sample, even at the same incident angle. After placing each sample onto the GIUSAXS sample stage, the position of the sample needs to be adjusted. Thus, the simplest GIUSAXS sample stage requires movement along at least two directions: one direction is vertical in order to adjust the sample to the proper height; the other one is to rotate the sample stage around the axis that is vertical to the incident X-ray beam in the horizontal plane, so that the angle towards the incident beamline can be regulated. In practice, another two move-

Figure 1
The designed GISAXS/GIUSAXS experimental platform based on a modified Xeuss apparatus.

ments are necessary for a better alignment. Therefore, the third movement direction is perpendicular to the X-ray beam in the horizontal plane. This direction of motion will be used to find the best position of the sample. The last adjustment direction is a rotation around the incident X-ray beam to obtain an untilted scattering pattern.

Fig. 1(*a*) shows the X-ray diffraction and scattering setup (modified Xeuss system, Xenocs) used for the current work. The X-rays are generated by a GeniX^{3D} type X-ray source coupled with FOX three-dimensional multilayer optics, producing a highly collimated beam with a divergence of 0.8 mrad (Fig. 1*b*). The diffracted/scattered signal from the sample is collected by a Pilatus 100K-S type area detector (Dectris Swiss) with a pixel size of 172 × 172 µm and a module size of 83.8 × 33.5 mm (Fig. 1*c*). In its standard configuration, the Xeuss system was equipped with two scatterless slit systems placed after the multilayer optics and before the sample stage. The two slit systems were separated by 1200 mm. The slits use single crystals to shape the beam so that parasitical scattering due to the crystalline grain boundaries in conventional metal blades is significantly reduced. Therefore, the normally needed third guard slit system or pinhole before the sample is no longer necessary in the Xeuss system. The major changes in our setup compared with the commercial Xeuss are an elongation of the collimating system, by increasing the distance between the two scatterless slit systems from 1200 to 2400 mm, and an elongated sample-to-detector distance, up to 6558 mm. In transmission mode, the modified setup reaches an ultra-small-angle regime suitable for investigating structural features up to several hundred nanometres, such as cavitation in semi-crystalline polymers during stretching (Wang *et al.*, 2014). The setup has been standardized as Xeuss 2.0 UHR. The designed GIUSAXS sample stage was placed at the sample holder position, replacing the standard sample holder. The X-ray photon counter (PIN diode detector, Xenocs) previously used for sample alignment was mounted at a custom-made holder behind the GIUSAXS stage, facing the incident X-ray beam.

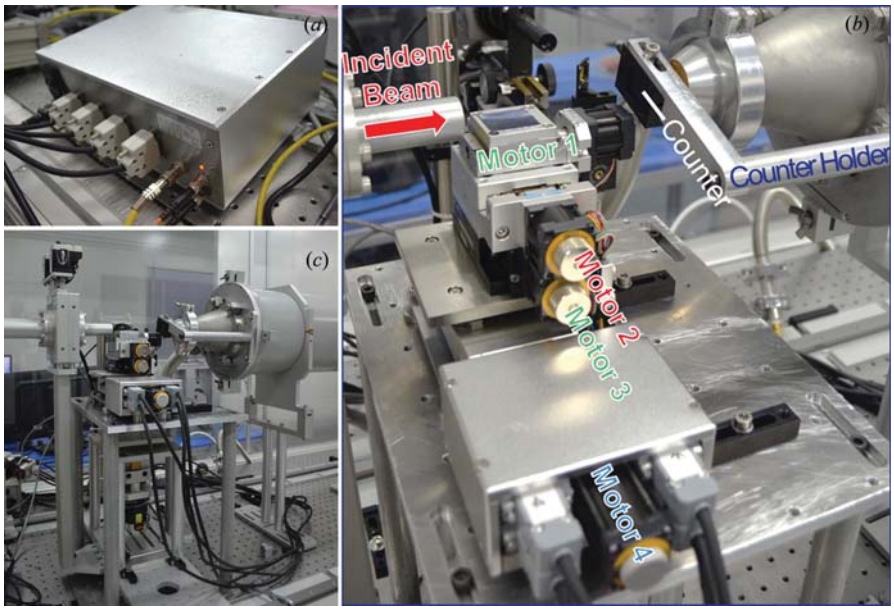

Figure 2
The designed GISAXS/GIUSAXS sample stage.

2.1.1. The design of the GIUSAXS sample stage. The designed GIUSAXS sample stage system consists of two main parts: the control center (Fig. 2*a*) and a motorized positioning sample stage (Fig. 2*b*). The motorized positioning sample stage is installed on an aluminium shelf (Fig. 2*c*). The control center connects the computer, the motorized positioning sample stage and the X-ray photon counter. It transmits the control signals from the computer's graphical user interface to the four motors in the sample stage. The electric power of the sample stages is also provided by the control center.

The motorized positioning sample stage is composed of four separate positioning stages driven by step motors. Two of them

Table 1
Parameters of the four motorized positioning stages.

					Positioning precision		
Channel	Units	Left limit	Right limit	Total steps	High	Medium	Low
1	°	−5	5	26000	0.0185	0.00308	0.00154
2	°	−5	5	10000	0.0180	0.0060	0.0030
3	mm	0	30	30000	0.0600	0.0300	0.0060
4	mm	0	6	12000	0.0150	0.0030	0.0015

are angle positioning stages, one is a horizontal positioning stage and the other one is a vertical positioning stage. As designed, the four step motors controlling the positioning stages enable the sample stage to move along different directions to adjust the sample to the proper position (see Fig. 2*b*). The parameters of these four motorized positioning stages are listed in Table 1.

Before a GIUSAXS measurement, the X-ray photon counter (see Fig. 2*b*) should be moved on the beamline to block and detect the incident X-ray beam to perform a height scan. A curve of intensity *versus* height should be obtained (Fig. 3*a*). Then, the height of the sample stage should be positioned to the point of half-intensity between the maximum and minimum, because of the existence of dark current of the counter. After that, an angle scanning must be performed to find the angle at which the intensity reaches its maximum (Fig. 3*b*). Repeat these two scanning processes until a repeatable position appears, which means that the right position for GIUSAXS measurement has been achieved. Then adjust the angle toward the beamline to a certain value. The GIUSAXS measurement can then be started.

3. Results

A polystyrene (PS) latex dispersion (14.09 wt%) was synthesized through emulsion polymerization using sodium dodecyl sulfate as surfactant, following the procedure reported in the literature (Ruhl *et al.*, 2004). The PS latex particles are 215 nm in diameter with a 3.89% size polydispersity according to a Gaussian distribution, as was determined by SAXS. A thin PS latex film was prepared for the GIUSAXS experiment as follows: 55 µl of 2 wt% PS latex dispersion was cast onto a silicon substrate with a size of 20 × 30 mm; then the silicon wafer was dried in a vacuum oven at room temperature. In this

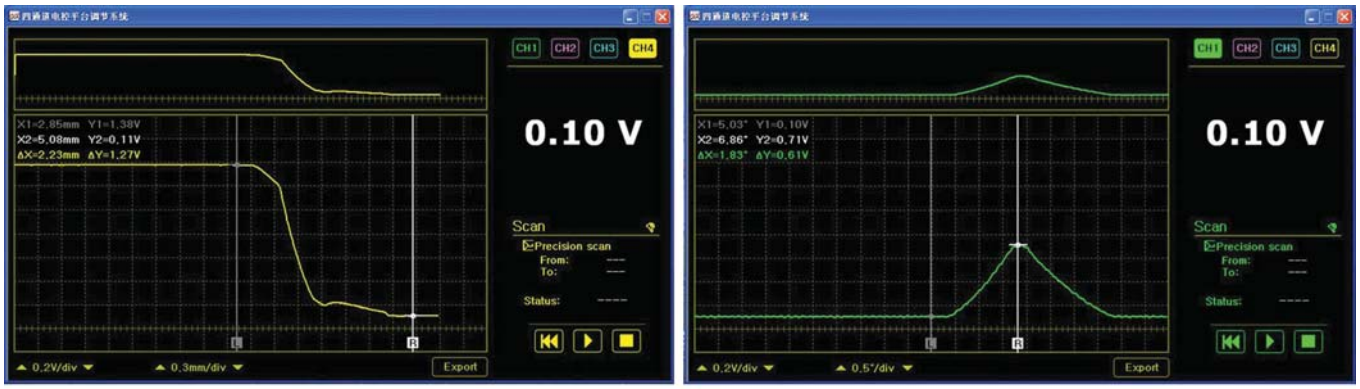

Figure 3
Graphic interface of the control software: height scan (*a*) and angle scan (*b*).

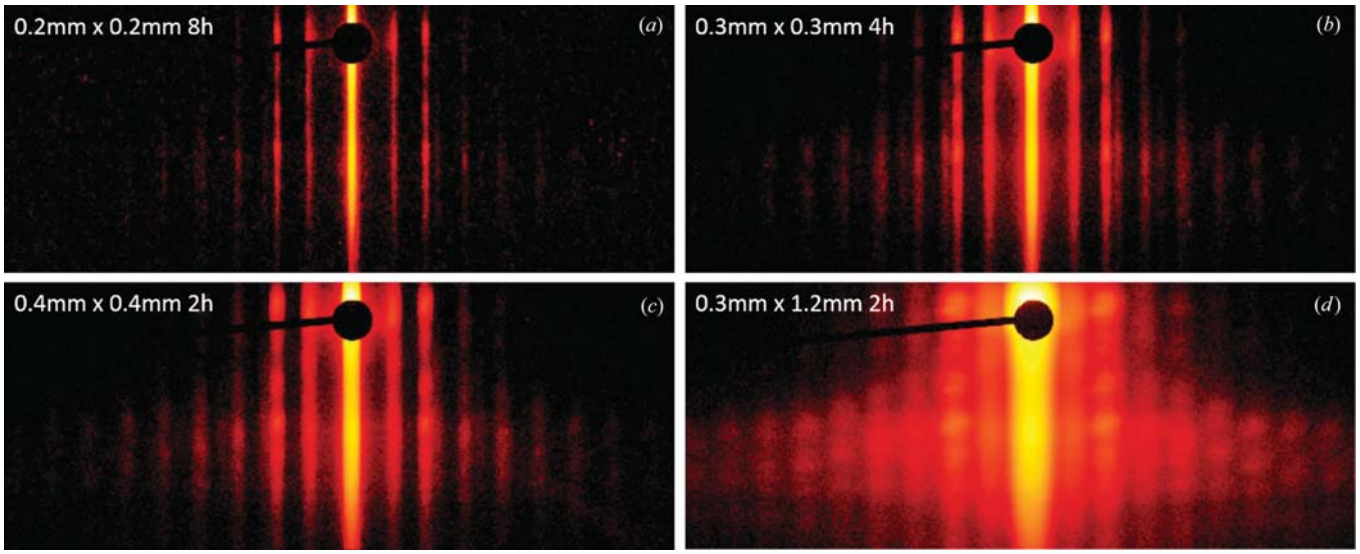

Figure 4
The two-dimensional GIUSAXS pattern from the designed grazing-incidence experimental platform. The sample-to-detector distance was 6558 mm.

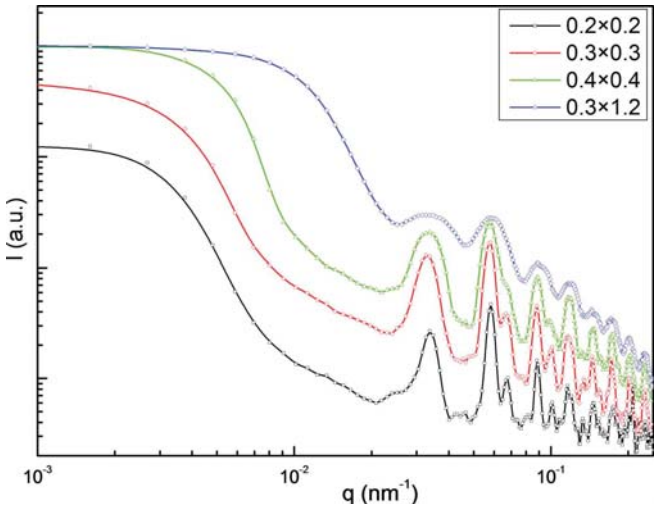

Figure 5
The one-dimensional GIUSAXS curves of GIUSAXS patterns integrated perpendicular to the Yoneda peak at different beam sizes.

case, the process of drying yields latex particles packed into a colloidal crystalline structure (Men, 2012). Taking advantage of the scatterless slit systems, we measured the sample under different beam sizes. Here the most important size is the horizontal opening of the slits, because of the large footprint of the beam at the current vertical slit opening. At a grazing-incidence angle of 0.26°, the footprint of the beam for a vertical slit opening of 0.2 mm is 44 mm, which already exceeds the width of the silicon wafer employed. The exposure time was extended while the beam size was decreased to ensure the intensity of the scattering signal. The two-dimensional GIUSAXS patterns are shown in Fig. 4. It can be seen from Fig. 4 that the scattering signals were smeared owing to the increase of horizontal beam size.

In order to observe the intensity distribution so that the microstructural features are clearly visible, one-dimensional intensity distribution curves were obtained *via* integration along the horizontal direction over the Yoneda peak in the GIUSAXS patterns shown in Fig. 4. The thus obtained one-dimensional curves are collected in Fig. 5. Several features can be read from Fig. 5. First of all, one observes a gradual smearing of the sharp diffraction peaks present under the condition of smallest beam size when the horizontal beam size is increased. Eventually, the curve ends up with several broad peaks at a horizontal beam size of 1.2 mm. Clearly, without prior knowledge of the fine crystalline structures of the sample, it is not possible to desmear the curve back to its theoretical values. Second, the smallest achievable scattering vector magnitude (q_{min}) for structure determination decreases with the decrease of horizontal beam size. At a horizontal beam size of 0.2 mm, q_{min} reaches 0.01 nm^{-1} easily. Notably, even at very small scattering vectors a considerable number of data points can be collected owing to the elongated sample-to-detector distance, making possible the measurement of structures of up to 600 nm.

To further explore the capability of the measurements in a colloidal crystalline structural determination, the one-dimensional curve obtained under the condition of beam size 0.2 × 0.2 mm was enlarged and is presented in Fig. 6. By assuming sphere packing, the diffraction peaks can be satisfactorily assigned to three colloidal crystalline structures, namely face-centered cubic (f.c.c.), body-centered cubic (b.c.c.) and hexagonal close packed (h.c.p.). Evidently, f.c.c. and h.c.p. crystalline structures are the dominant ones, whereas only a small fraction of b.c.c. crystallites are present in the system.

Although current application examples of our laboratory GIUSAXS setup present static structural analysis, one could also consider the possibility of kinetic measurements for those systems possessing much higher electron density contrast, such as an assembly of metal nanoparticles. Furthermore, such kinetic measurements on systems of high electron density contrast can be better realized when the desired structure falls into the GISAXS regime, as the detected scattering intensity scales to the square of the sample-to-detector distance.

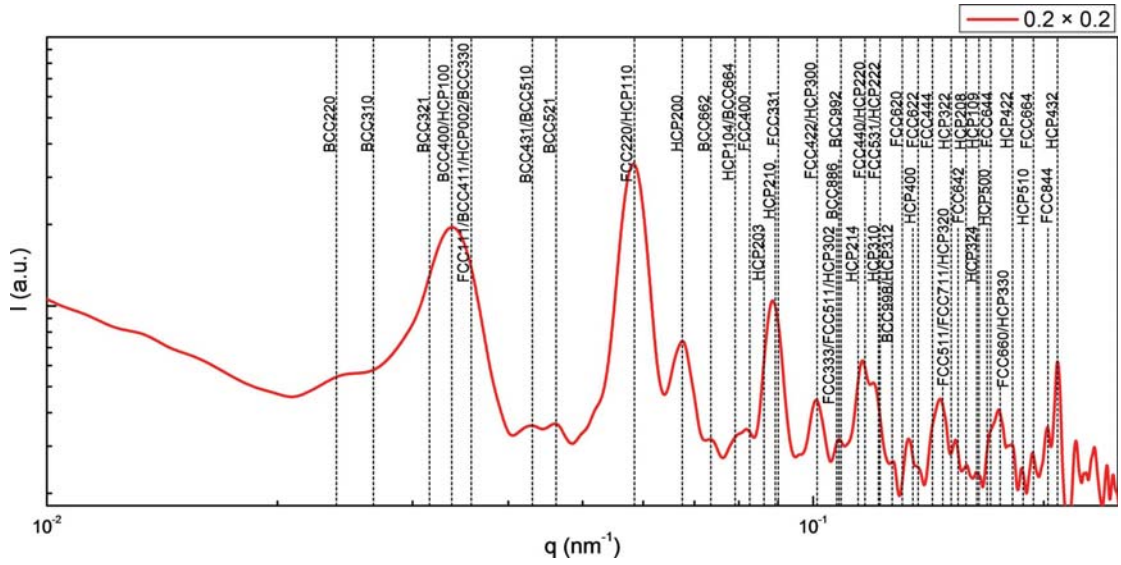

Figure 6
The analysis of colloidal crystalline structures of the PS latex film based on the GIUSAXS one-dimensional curve from the designed GIUSAXS experimental platform with a beam size of 0.2 × 0.2 mm.

4. Conclusions

GIUSAXS measurements have been successfully performed in a modified Xeuss system (Xenocs) by increasing both the distance between the collimating slit systems and the sample-to-detector distance. A custom-designed and -assembled grazing-incidence sample stage allows precise positioning of the thin-film samples to be measured in grazing-incidence geometry. Such a sample stage could also be used for future grazing-incidence small- and wide-angle X-ray scattering experiments. The reciprocal spatial resolution of the designed GIUSAXS experimental platform increases with the reduction of X-ray beam size. At a beam size of 0.2×0.2 mm, the smallest achievable scattering vector magnitude reaches 0.01 nm^{-1} with still a considerable number of data points available. As an example, we collected GIUSAXS patterns of a thin latex film, obtained by vacuum drying a cast PS latex dispersion on a silicon wafer, at different beam size settings. The critical role of the beam size smearing effect was illustrated. From the high-resolution GIUSAXS result, one is able to conclude that different amounts of f.c.c., b.c.c. and h.c.p. colloidal crystalline order coexist in the prepared PS latex film.

This work was supported by the National Natural Science Foundation of China (No. 21074136) and the National Basic Research Program of China (No. 2012CB821500). The work of NZ, ZY and RC forms part of the research programme of the DPI, project No. 779.

References

Altamura, D., De Caro, L., Corricelli, M., Falqui, A., Striccoli, M., Curri, M. L. & Giannini, C. (2012). *Cryst. Growth Des.* **12**, 1970–1976.
Altamura, D., Holy, V., Siliqi, D., Lekshmi, I. C., Nobile, C., Maruccio, G., Cozzoli, P. D., Fan, L. X., Gozzo, F. & Giannini, C. (2012). *Cryst. Growth Des.* **12**, 5505–5512.
Altamura, D., Lassandro, R., Vittoria, F. A., De Caro, L., Siliqi, D., Ladisa, M. & Giannini, C. (2012). *J. Appl. Cryst.* **45**, 869–873.
Altamura, D., Sibillano, T., Siliqi, D., De Caro, L. & Giannini, C. (2012). *Nanomater. Nanotechnol.* **2**, 1–23.
Cheng, W. D., Mo, G., Xing, X. Q., Wang, D. H., Gong, Y., Cai, Q., Chen, Z. J. & Wu, Z. H. (2011). *Chin. Phys. C*, **35**, 875–879.
De Caro, L., Altamura, D., Vittoria, F. A., Carbone, G., Qiao, F., Manna, L. & Giannini, C. (2012). *J. Appl. Cryst.* **45**, 1228–1235.
Di, Z. Y., Posselt, D., Smilgies, D. M., Li, R. P., Rauscher, M., Potemkin, I. I. & Papadakis, C. M. (2010). *Macromolecules*, **43**, 418–427.
Holy, V. & Baumbach, T. (1994). *Phys. Rev. B*, **49**, 10668–10676.
Hu, S. S., Rieger, J., Roth, S. V., Gehrke, R., Leyrer, R. J. & Men, Y. F. (2009). *Langmuir*, **25**, 4230–4234.
Jergel, M., Šiffalovič, P., Végsö, K., Majková, E., Korytár, D., Zápražný, Z., Perlich, J., Ziberi, B., Cornejo, M. & Vagovic, P. (2013). *J. Appl. Cryst.* **46**, 1544–1550.
Levine, J. R., Cohen, J. B., Chung, Y. W. & Georgopoulos, P. (1989). *J. Appl. Cryst.* **22**, 528–532.
Li, Z. H., Wu, Z. H., Mo, G., Xing, X. Q. & Liu, P. (2014). *Instrum. Sci. Technol.* **42**, 128–141.
Magliulo, M., Altamura, D., Di Franco, C., Santacroce, M. V., Manoli, K., Mallardi, A., Palazzo, G., Scamarcio, G., Giannini, C. & Torsi, L. (2014). *J. Phys. Chem. C*, **118**, 15853–15862.
Mele, E., Lezzi, F., Polini, A., Altamura, D., Giannini, C. & Pisignano, D. (2012). *J. Mater. Chem.* **22**, 18051–18056.
Men, Y. F. (2012). *Soft Matter*, **8**, 5723–5727.
Müller-Buschbaum, P. (2003). *J. Phys. Condens. Matter*, **15**, R1549–R1582.
Müller-Buschbaum, P., Casagrande, M., Gutmann, J., Kuhlmann, T., Stamm, M., von Krosigk, G., Lode, U., Cunis, S. & Gehrke, R. (1998). *Europhys. Lett.* **42**, 517–522.
Müller-Buschbaum, P., Gutmann, J. S., Lorenz-Haas, C., Wunnicke, O., Stamm, M. & Petry, W. (2002). *Macromolecules*, **35**, 2017–2023.
Müller-Buschbaum, P., Gutmann, J. S. & Stamm, M. (1999). *Phys. Chem. Chem. Phys.* **1**, 3857–3863.
Müller-Buschbaum, P., Gutmann, J. S., Stamm, M., Cubitt, R., Cunis, S., von Krosigk, G., Gehrke, R. & Petry, W. (2000). *Physica B*, **283**, 53–59.
Müller-Buschbaum, P. & Stamm, M. (1998). *Macromolecules*, **31**, 3686–3692.
Naudon, A. & Thiaudiere, D. (1997). *J. Appl. Cryst.* **30**, 822–827.
Ogawa, H., Miyazaki, T., Shimokita, K., Fujiwara, A., Takenaka, M., Yamada, T., Sugihara, Y. & Takata, M. (2013). *J. Appl. Cryst.* **46**, 1610–1615.
Papadakis, C. M., Di, Z. Y., Posselt, D. & Smilgies, D. M. (2008). *Langmuir*, **24**, 13815–13818.
Renaud, G., Lazzari, R. & Leroy, F. (2009). *Surf. Sci. Rep.* **64**, 255–380.
Roth, S. V., Autenrieth, T., Grubel, G., Riekel, C., Burghammer, M., Hengstler, R., Schulz, L. & Müller-Buschbaum, P. (2007). *Appl. Phys. Lett.* **91**, 091915.
Roth, S. V., Burghammer, M., Riekel, C., Muller-Buschbaum, P., Diethert, A., Panagiotou, P. & Walter, H. (2003). *Appl. Phys. Lett.* **82**, 1935–1937.
Roth, S. V., Döhrmann, R., Dommach, M., Kuhlmann, M., Kröger, I., Gehrke, R., Walter, H., Schroer, C., Lengeler, B. & Müller-Buschbaum, P. (2006). *Rev. Sci. Instrum.* **77**, 085106.
Ruhl, T., Spahn, P., Winkler, H. & Hellmann, G. P. (2004). *Macromol. Chem. Phys.* **205**, 1385–1393.
Russell, T. P. (2002). *Science*, **297**, 964–967.
Salditt, T., Metzger, T. H., Peisl, J. & Goerigk, G. (1995). *J. Phys. D*, **28**, A236–A240.
Wang, Y. T., Jiang, Z. Y., Fu, L. L., Lu, Y. & Men, Y. F. (2014). *PLoS ONE*, **9**, e97234.
You, J. C., Liao, Y. G., Men, Y. F., Shi, T. F., An, L. J. & Li, X. H. (2011). *Macromolecules*, **44**, 5318–5325.
Zhang, J. Q., Posselt, D., Sepe, A., Shen, X. H., Perlich, J., Smilgies, D. M. & Papadakis, C. M. (2013). *Macromol. Rapid Commun.* **34**, 1289–1295.
Zhang, J. Q., Posselt, D., Smilgies, D. M., Perlich, J., Kyriakos, K., Jaksch, S. & Papadakis, C. M. (2014*a*). *Macromolecules*, **47**, 5711–5718.
Zhang, J. Q., Posselt, D., Smilgies, D. M., Perlich, J., Kyriakos, K., Jaksch, S. & Papadakis, C. M. (2014*b*). *Macromol. Rapid Commun.* **35**, 1622–1629.
Zhao, N., Yang, C. M., Zhang, Q., Lu, X. M., Wang, Y. Z. & Wang, J. (2014). *J. Appl. Phys.* **115**, 204311.
Zhong, Q., Metwalli, E., Rawolle, M., Kaune, G., Bivigou-Koumba, A. M., Laschewsky, A., Papadakis, C. M., Cubitt, R. & Müller-Buschbaum, P. (2013). *Macromolecules*, **46**, 4069–4080.
Zhong, Q., Wang, W. N., Adelsberger, J., Golosova, A., Koumba, A. M. B., Laschewsky, A., Funari, S. S., Perlich, J., Roth, S. V., Papadakis, C. M. & Müller-Buschbaum, P. (2011). *Colloid Polym. Sci.* **289**, 569–581.